QUANTUM MAGNETISM

Revealing hidden antiferromagnetic correlations in doped Hubbard chains via string correlators

Timon A. Hilker,[1]* Guillaume Salomon,[1] Fabian Grusdt,[2] Ahmed Omran,[1]† Martin Boll,[1] Eugene Demler,[2] Immanuel Bloch,[1,3] Christian Gross[1]

Topological phases, like the Haldane phase in spin-1 chains, defy characterization through local order parameters. Instead, nonlocal string order parameters can be employed to reveal their hidden order. Similar diluted magnetic correlations appear in doped one-dimensional lattice systems owing to the phenomenon of spin-charge separation. Here we report on the direct observation of such hidden magnetic correlations via quantum gas microscopy of hole-doped ultracold Fermi-Hubbard chains. The measurement of nonlocal spin-density correlation functions reveals a hidden finite-range antiferromagnetic order, a direct consequence of spin-charge separation. Our technique, which measures nonlocal order directly, can be readily extended to higher dimensions to study the complex interplay between magnetic order and density fluctuations.

The Fermi-Hubbard model, describing systems of strongly correlated fermions on a lattice, lies at the heart of our understanding of the Mott insulator–metal transitions and quantum magnetism (*1*). The complexity of the interplay between hole doping and magnetic ordering in this model is believed to give rise to a rich phase diagram, including a high-Tc superconducting phase as, for example, observed in cuprate compounds (*2*). In one spatial dimension, however, the competition between the spin and density sectors is largely absent owing to the separation of the spin and density modes at low energy. This phenomenon of spin-charge separation, generally appearing in Luttinger liquids, is well understood theoretically (*3*), but there are only limited experimental observations. Existing experimental evidence is based on spectroscopic (*4*–*6*) or transport measurements (*7*, *8*) in condensed-matter systems. When the quasi–long-range antiferromagnetic order at zero temperature is measured by two-point spin correlation functions, it appears to be suppressed by a finite hole density in the system. However, thanks to the independence of the spin and charge sectors, the order is not truly reduced, but rather hidden (*9*–*11*). It can be revealed by measurements over an extensive part of the system, allowing one to construct string correlation functions. In analogy to the spin-1 Haldane phase (*12*–*14*), this requires measuring all spins in the chain. A closely related way to unveil the hidden order is to work directly in "squeezed space," where empty sites are completely removed from the system (*15*–*18*). In traditional condensed-matter systems, string order cannot be measured, nor is squeezed space accessible to experiments. Fermionic quantum gas microscopes (*19*–*24*), by contrast, provide access to snapshots of the full spin and density distribution with single-site resolution (*25*), such that nonlocal correlation functions can be extracted (*26*). Here we report on the direct measurement of string correlations in ultracold Fermi-Hubbard chains. The ability to locally detect holes, doublons, and the spin state allows for an analysis of the system directly in squeezed space, in which Heisenberg spin correlations are restored (*18*). Our observations provide a microscopic picture of spin-charge separation independent of the more frequently discussed spectral properties or the excitation dynamics.

We probed the physics of the doped one-dimensional Fermi-Hubbard model using a balanced spin mixture of ^{6}Li trapped in a single plane of a two-dimensional optical lattice. A versatile quantum gas microscope allowed for the simultaneous local detection of both spin states (*25*) (Fig. 1A). By controlling the lattices depths in the different spatial directions (*27*), we created independent one-dimensional systems described by the single-band Hubbard Hamiltonian

$$\hat{H} = -t\sum_{i,\sigma}(\hat{c}^{\dagger}_{i,\sigma}\hat{c}_{i+1,\sigma} + h.c.) + U\sum_{i}\hat{n}_{i,\uparrow}\hat{n}_{i,\downarrow} + \sum_{i,\sigma}\varepsilon_i\hat{n}_{i,\sigma} \quad (1)$$

The fermion creation (annihilation) operator is denoted by $\hat{c}^{\dagger}_{i,\sigma}$ ($\hat{c}_{i,\sigma}$) at site i for each of the two spin states $\sigma = \uparrow, \downarrow$ and the operator $\hat{n}_{i,\sigma} = \hat{c}^{\dagger}_{i,\sigma}\hat{c}_{i,\sigma}$ counts the number of atoms with spin σ at site i. The energy offsets ε_i result from an additional confinement caused by the lattice beams, which leads to a smoothly changing local density $n_i = \langle\hat{n}_i\rangle = \langle\hat{n}_{i,\uparrow} + \hat{n}_{i,\downarrow}\rangle$. At half filling in the strong coupling limit ($U/t \gg 1$), the Fermi-Hubbard model reduces to a Heisenberg spin chain with $J = 4t^2/U$ and supports quasi–long-range antiferromagnetic (AFM) order at zero temperature (*1*). The doped system is described at long wavelength by Luttinger liquid theory, which predicts at zero temperature an algebraic decay of the spin correlations with distance that is faster than the one of the Heisenberg model (*3*). This decay can be understood from spin-charge separation, allowing holes to freely move in the AFM spin-chain. Consequently, the spins around the hole are anti-aligned, and the sign of the staggered magnetization $(-1)^i S^z_i$, called AFM parity, changes. This implies that a hole acts as a domain wall of the AFM parity, which reduces the spin correlations. The spin order, however, is still present and can be revealed either in squeezed space by effectively removing the holes in the analysis or by evaluating string correlators, which take the AFM parity domain walls into account by flipping the sign of the correlator (Fig. 1C). Analytic and numerical studies (*18*) have shown that at zero temperature, the two-point spin correlations in squeezed space are comparable to the ones of a pure Heisenberg chain, for any doping and any repulsive interaction U. This is readily understood in the $U/t\to\infty$ limit, where the many-body wave function $\Psi(\{x_{j,\sigma}\}) = \Psi_{ch}(\{x_j\})\Psi_s(\{\tilde{x}_{j,\sigma}\})$ factorizes exactly into a density Ψ_{ch} and a spin Ψ_s part (*15*, *28*). The spin degree of freedom is described by a Heisenberg model in squeezed space with the spins "living" on a lattice defined by the positions of spinless, noninteracting fermions (*16*). Distances in squeezed space $\tilde{x} = x - N_h$ are shorter by the number of holes within this distance N_h, leading on average to a rescaling by the spinless fermion density $\tilde{x} \sim nx$. Even at nonzero temperature and finite interactions, the spin correlations in squeezed space are governed by a Heisenberg model with a renormalized exchange coupling $J_{\mathrm{eff}}(n)$ that depends on the original density n (*27*).

The experiment started with a two-dimensional degenerate two-component Fermi gas. Using the large spacing component of an optical superlattice ($a_{sl} = 2.3\mu$m), we divided the system into about 10 independent one-dimensional tubes. The Fermi Hubbard chains were then realized with a lattice of 1.15-μm spacing along the tubes. The atom number was set such that the maximum density in the chains was typically just below unity. At the end of the lattice ramps, the tunneling amplitude reached $t = h \times 400$ Hz, and the confinement caused by the lattice beams fixed the length of the central tubes to about 15 sites. The onsite repulsion U was tuned to $h \times 2.9$ kHz using the broad Feshbach resonance between the hyperfine states $|\downarrow\rangle = |F, m_F\rangle = |1/2, -1/2\rangle$ and $|\uparrow\rangle = |1/2, 1/2\rangle$ to set a scattering length of 2000 Bohr radii at the end of the lattice ramps, resulting in an exchange interaction of $J = h \times 220$ Hz. These parameters and the lattice ramps have been optimized to produce cold, strongly interacting doped Hubbard chains (*27*). For the detection of the spin and density degrees of freedom, the lattice depth along the tubes was rapidly increased, followed by a local Stern-Gerlach–like detection with a magnetic field

[1]Max-Planck-Institut für Quantenoptik, 85748 Garching, Germany. [2]Department of Physics, Harvard University, Cambridge, MA 02138, USA. [3]Fakultät für Physik, Ludwig-Maximilians-Universität, 80799 München, Germany.
*Corresponding author. Email: timon.hilker@mpq.mpg.de
†Present address: Department of Physics, Harvard University, Cambridge, MA 02138, USA.

gradient and the short-scale component of a superlattice transverse to the tubes (*25*). Applying Raman sideband cooling for 500 ms, we collected fluorescence photons on an EMCCD (electron multiplying charge-coupled device) camera to form a high-contrast and site-resolved image of the atomic distribution (*22*) (Fig. 1A). Following our analysis in (*25*), we estimated the temperature in the central chains to be $0.51(2)\,t$ or $0.90(3)\,J$, which corresponds to an entropy per particle of $0.63(2)k_B$ (where k_B is the Boltzmann constant).

To investigate the magnetic environment around a hole, we calculate the conditional three-point spin-hole correlation function $C_{SH}(2) = 4\langle \hat{S}^z_i \hat{S}^z_{i+2} \rangle_{\bullet_i \circ_{i+1} \bullet_{i+2}}$, where the symbols describe the condition that the correlator is evaluated only on configurations with the sites i and $i+2$ singly occupied and the middle site empty (*27*). The correlator indeed reveals anti-alignment of the spins around individual holes [$C_{SH}(2) < 0$], and Fig. 2A highlights the hole-induced sign change by comparison to the standard two-point correlator $C(d) = 4(\langle \hat{S}^z_i \hat{S}^z_{i+d} \rangle_{\bullet_i \bullet_{i+d}} - \langle \hat{S}^z_i \rangle_{\bullet_i} \langle \hat{S}^z_{i+d} \rangle_{\bullet_{i+d}})$ of an undoped spin chain. To obtain unity filling, the latter was evaluated on a hole-free subset of the data. The additional condition indicated by the filled circular symbols removes the trivial n^2 density dependence of the two-point spin correlator in the doped case (*27*) but has no effect at unity filling. The measured modulus of the correlation around a hole is $|C_{SH}(2)| = 0.184(4)$, considerably larger than $C(2) = 0.057(3)$ and about half of the next-neighbor value of $|C(1)| = 0.316(2)$. At zero temperature for $U/t \to \infty$ one expects $|C_{SH}(2)| = |C(1)|$, as the hole has no effect on the magnetic alignment of its surrounding spins. For our interaction strength, the measured difference agrees with exact diagonalization results at a temperature $0.94(5)\,J$ (*27*). These calculations take into account the experimental fluctuations of the magnetization per chain. Because of finite size effects, the correlation function shows a small offset at large distances, for which we correct in the subsequent analysis throughout this paper (*27*).

The influence of larger doping on the spin order is revealed by studying $C_{SH}(d)$ as a function of the number of holes between the two spins; that is, by evaluating $C_{SH,N_h}(d) = 4\langle \hat{S}^z_i \hat{S}^z_{i+d} \rangle_{\bullet_i \{\circ\}_{N_h} \bullet_{i+d}}$ with exactly N_h holes on the otherwise singly occupied string of length $d+1$. The results of this analysis, shown in Fig. 2B, reveal a sign change of C_{SH,N_h} at fixed distance d for each newly introduced hole and antiferromagnetic correlations versus distance for fixed hole number N_h. Thus, each hole indeed corresponds to a flip of the antiferromagnetic parity. In a thermodynamic ensemble, the hole number between the two measured spins fluctuates, resulting in a weighted averaging over the alternating correlations for different hole numbers. This directly explains the suppression of magnetic correlations with hole doping (compare Fig. 3A).

The strong reduction in the amplitude of spin correlations caused by hole fluctuations does not imply the absence of magnetic order in the system, but rather suggests that it is hidden by the fluctuations in the position of the atoms. This situation is similar to the Haldane phase of spin-1 chains (*9*, *12*–*14*), where fluctuating $|0\rangle$ spins hide correlations between the $|\pm 1\rangle$ components, leading to exponentially decaying local correlators. The intrinsic AFM order is unveiled by considering a nonlocal correlation function. By identifying double occupancies and holes with spin $|0\rangle$ states, one can use the same procedure to construct a string correlator that probes the underlying spin order in the doped Hubbard chain(*18*):

$$C^{str}(d) = 4\left\langle \hat{S}^z_i \left(\prod_{j=1}^{d-1} (-1)^{(1-\hat{n}_{i+j})} \right) \hat{S}^z_{i+d} \right\rangle_{\bullet_i \bullet_{i+d}} \quad (2)$$

This string correlator takes the antiferromagnetic parity flips into account by a corresponding sign flip for each hole (compare Fig. 1C). The unique ability to detect the spin and density locally on single images (*25*) enables the direct

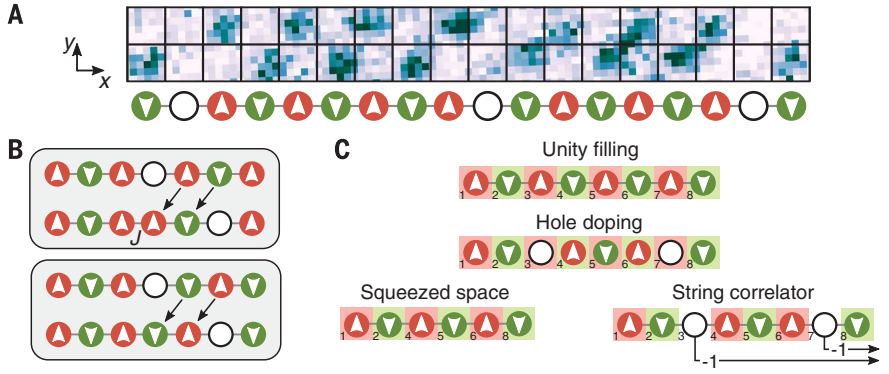

Fig. 1. Analysis of a doped Hubbard chain. (**A**) Experimental spin and density-resolved image of a single, slightly doped Hubbard chain after a local Stern-Gerlach-like detection. The reconstructed chain is shown below the picture. (**B**) Illustration of the magnetic environment around a hole. For aligned spins (top) the hole cannot freely delocalize because of the magnetic energy cost J, which is absent for anti-aligned spins (bottom). (**C**) Illustration of hole-induced AFM parity flips, squeezed space, and string correlator. Hole doping leads to AFM parity flips highlighted by the color mismatch between the spins and the background (top). Squeezed space is constructed by removing all sites with holes from the chain (bottom left). In the string correlator analysis, the flip in the AFM parity is canceled by a multiplication of –1 for each hole (bottom right). Comparing either of these analyses to the conventional two-point correlator reveals the hidden finite-range AFM order in the system.

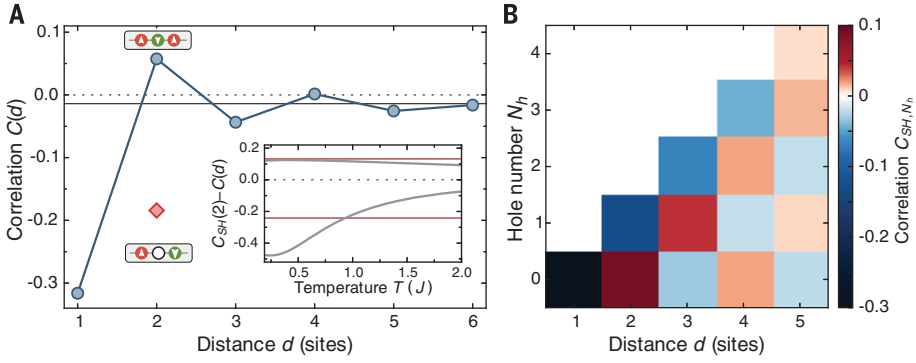

Fig. 2. Revealing the magnetic environment around holes. (**A**) Connected two-point spin correlation function $C(d)$ analyzed on occupied sites only (blue). The finite-range AFM order without holes asymptotically falls off with an exponential decay length of 1.3(2) sites. The spin correlations at a distance of two sites switch sign in the presence of a hole as measured by $C_{SH}(2)$ (red diamond) demonstrating an AFM environment surrounding the hole. The solid black line indicates the finite-size offset (*27*), the blue line is a guide to the eye, and statistical uncertainties are smaller than the symbol sizes. (Inset) Comparison of experimental values (red lines) of $C_{SH}(2) - C(1)$ (top) and $C_{SH}(2) - C(2)$ (bottom) with finite temperature results from exact diagonalization (gray curves). The systematic error originating from a finite atom loss rate of up to 3% during imaging is negligible. (**B**) Amplitude of the correlation function $C_{SH,N_h}(d)$ as a function of distance d and the number of holes N_h between the two spins with the finite-size offset subtracted. The parity of the AFM order flips with every hole.

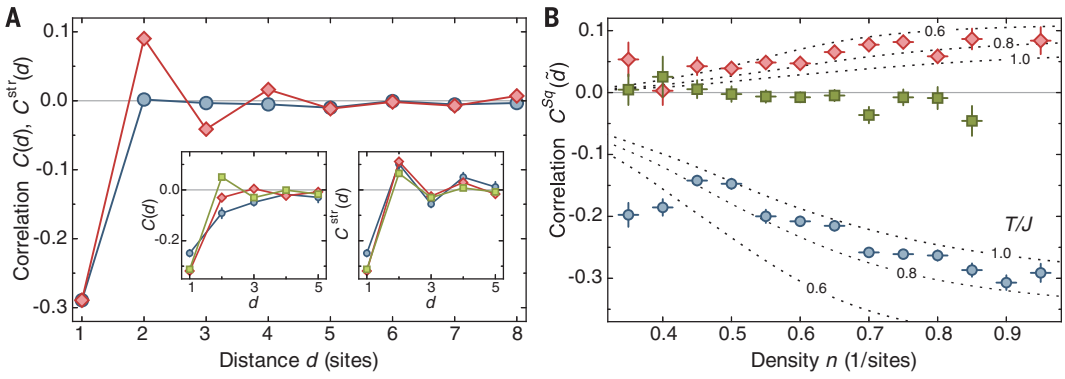

Fig. 3. Effect of hole doping on spin order. (**A**) Comparison of the spin correlation function (blue) $C(d)$ and the spin-string correlation function (red) $C^{str}(d)$ averaged over all local densities in the trap. The spin order is not visible with the conventional two-point spin correlator, but can be revealed by disentangling spin and charge sector with the string correlator. The extracted exponential decay length of 1.2(1) sites matches the one extracted at unity filling (compare Fig. 1). The insets show the data binned by density (bin widths 0.1) for $\langle n\rangle = 0.4$ (blue), $\langle n\rangle = 0.7$ (red), and $\langle n\rangle = 1$ (green). Finite-range AFM order in the conventional correlator $C(d)$ is present at $\langle n\rangle = 1$, whereas it quickly gets suppressed when the system is doped away from half filling. At the same time, we observe a decreasing wave vector of the oscillations shown by the two-point spin correlations with decreasing density (left). By contrast, string correlations $C^{str}(d)$ only marginally depend on density (right). Solid lines are guides to the eye. (**B**) Spin correlation measured directly in squeezed space for $\tilde{d} = 1$ (blue), $\tilde{d} = 2$ (red), and $\tilde{d} = 3$ (green) as a function of density n (bin widths 0.05). Dotted lines represent spin correlations $C(1)$ and $C(2)$ in the Heisenberg model for temperatures $T/J = 0.6, 0.8, 1.0$ obtained by exact diagonalization with a coupling constant $J_{\mathrm{eff}}(n)$. The correlation decreases with increasing ratio $T/J_{\mathrm{eff}}(n)$. All correlations shown are corrected for the constant finite-size offset (*27*).

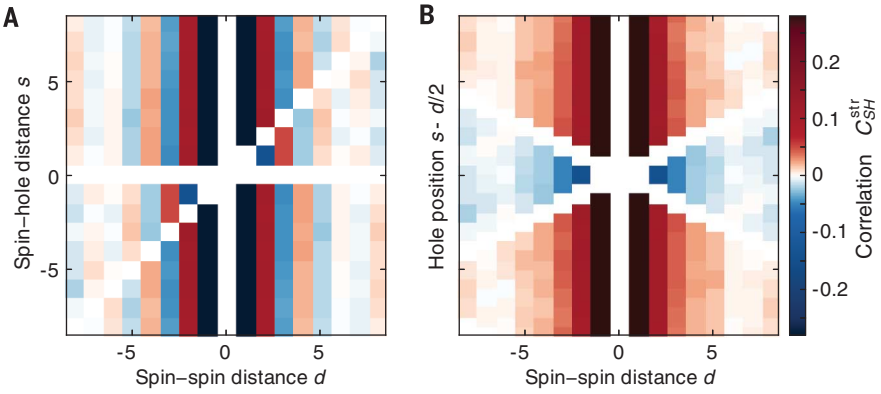

Fig. 4. Single holes as domain walls for the AFM order. (**A**) Tailored string correlator $C^{\mathrm{str}}_{\mathrm{SH}}(d,s)$ measuring the effect of a single hole on the doped Hubbard-chain. As expected for separated spin and charge sectors, the correlations are independent of the distance s between the hole and the spin, except for the opposite sign when the hole sits in between the two spins at relative distance d. In addition, there is a dynamic picture to the measurements shown here. Interpreting the vertical axis as time, one obtains the picture of a delocalized hole freely propagating through an antiferromagnetic background. The correlator $C^{\mathrm{str}}_{\mathrm{SH}}(d,s)$ is set to zero whenever two operators are evaluated at the same site. (**B**) Rectified correlator $(-1)^d\, C^{\mathrm{str}}_{\mathrm{SH}}(d, s - d/2)$ with hole position referenced to the string center. The hole-associated AFM parity flips are directly visible by the different domains. The expected parity is observed consistently for spin-spin distances of up to eight sites. The point symmetry around the origin is by construction of the correlator.

measurement of the string correlator $C^{str}(d)$ for different densities. The dependence of the string correlator on distance reported in Fig. 3A is in stark constrast with the standard two-point spin correlation function $C(d)$. Whereas $C(d)$ quickly vanishes when the data are analyzed over different densities, staggered correlations at distances up to four sites are detected with the string correlator $C^{str}(d)$ (Fig. 3A). When binning the data in regions of fixed density, we additionally observe a decreasing wave vector of the AFM correlations with decreasing density, as expected owing to the larger mean particle distance (*3*). The amplitude of the string correlations, by contrast, even slightly increase in magnitude with doping at a given real space distance d, which we attribute to the decreasing distance $\tilde{d} \sim nd$ in squeezed space (*27*).

An analysis of the correlations directly in squeezed space is also possible with the quantum gas microscope, by removing the empty and doubly occupied sites in the analysis before evaluating the standard two-point correlator $C(d)$. This corresponds to a weighted summation along the diagonals of Fig. 2B, and thus mixes events that had different distances in real space. Similar to the string correlator, the squeezed-space analysis (Fig. 3B) reveals the finite-range hidden antiferromagnetic order. A quantitative comparison to a Heisenberg model with renormalized coupling $J_{\mathrm{eff}}(n)$ that decreases with doping agrees well at a temperature of $T = 0.87(2)J$, which demonstrates that the concept of squeezed space can be successfully applied even away from the $U/t \to \infty$ limit (*29*). Here, J_{eff} was determined independently from the microscopic parameters of the Hubbard model (*27*). The discrepancy between theory and experiments at densities below the density of 0.45 might arise from adiabatic cooling when decreasing the density during the preparation of the chains.

To further confirm the independence of the spin and density sectors, we define a tailored string correlator $C^{\mathrm{str}}_{\mathrm{SH}}(d,s) = 4\left\langle \hat{S}^z_i \left(\prod_{j=1,j\neq s}^{d-1} (-1)^{(1-\hat{n}_{i+j})} \right) \hat{S}^z_{i+d} \right\rangle_{\bullet_i \circ_{i+s} \bullet_{i+d}}$, which isolates the effect of a single hole at distance s from the first spin independent of the density. Here, the effect of extra charge fluctuations is addressed by inserting string correlators around the hole. For a system with a single hole, this correlator is identical to the three-point correlation function introduced before $C^{\mathrm{str}}_{\mathrm{SH}}(d = 2, s = 1) = C_{\mathrm{SH}}(2)$. The dependence of $C^{\mathrm{str}}_{\mathrm{SH}}(d,s)$ on the spin separation d and the position of the hole in the string s is shown in Fig. 4A. For $s = 0$ and $s = d$, the hole crosses one of the two spins, which causes the previously discussed AFM parity flip, whereas the correlation signal is almost independent of the position of the hole between the two spins. This observation emphasizes spin-charge separation by the absence of polaron-like effects, which would result in a local change of the spin correlations around the hole. The rectified correlator $(-1)^d C^{\mathrm{str}}_{\mathrm{SH}}(d,s)$ in Fig. 4B highlights the two domains of opposite AFM parity, demonstrating that the hole acts as a domain wall for the magnetic order (*30*). To emphasize the symmetries of the three-point correlator, the position of the hole is

measured here relative to the center of mass of the two spins.

Through the analysis of various local and nonlocal correlation functions, our measurements revealed striking equilibrium signatures of spin-charge separation in one-dimensional Hubbard chains. An interesting extension of this work would be the detection of dynamic signatures of spin-charge separation in quench experiments through the measurements of different spin and charge velocities (*31*, *32*) or Green's function (*33*). In higher dimensions, the experimental evaluation of nonlocal correlations in synthetic hole-doped antiferromagnetic materials is also of prime interest for the investigation of exotic many-body phases relevant to high-temperature superconductors (*34*, *35*). The extension to two-dimensional frustrated quantum magnets would, for example, enable the detection of deconfined criticality through Wilson loops (*36*). Hence, our experiments mark a first step toward experimental studies of emergent gauge structures and topological order (*37*), such as those occurring in integer spin chains (*13*).

REFERENCES AND NOTES

1. A. Auerbach, *Interacting Electrons and Quantum Magnetism* (Springer Science and Business Media, 1994).
2. P. A. Lee, N. Nagaosa, X.-G. Wen, *Rev. Mod. Phys.* **78**, 17–85 (2006).
3. T. Giamarchi, *Quantum Physics in One Dimension* (Clarendon Press, 2004).
4. C. Kim *et al.*, *Phys. Rev. Lett.* **77**, 4054–4057 (1996).
5. P. Segovia, D. Purdie, M. Hengsberger, Y. Baer, *Nature* **402**, 504–507 (1999).
6. B. J. Kim *et al.*, *Nat. Phys.* **2**, 397–401 (2006).
7. O. M. Auslaender *et al.*, *Science* **308**, 88–92 (2005).
8. Y. Jompol *et al.*, *Science* **325**, 597–601 (2009).
9. M. den Nijs, K. Rommelse, *Phys. Rev. B Condens. Matter* **40**, 4709–4734 (1989).
10. T. Kennedy, H. Tasaki, *Phys. Rev. B Condens. Matter* **45**, 304–307 (1992).
11. H. V. Kruis, I. P. McCulloch, Z. Nussinov, J. Zaanen, *Europhys. Lett.* **65**, 512–518 (2004) (EPL).
12. F. Haldane, *Phys. Lett. A* **93**, 464–468 (1983).
13. F. D. M. Haldane, *Phys. Rev. Lett.* **50**, 1153–1156 (1983).
14. I. Affleck, T. Kennedy, E. H. Lieb, H. Tasaki, *Phys. Rev. Lett.* **59**, 799–802 (1987).
15. M. Ogata, H. Shiba, *Phys. Rev. B Condens. Matter* **41**, 2326–2338 (1990).
16. Y. Ren, P. W. Anderson, *Phys. Rev. B Condens. Matter* **48**, 16662–16672 (1993).
17. J. Zaanen, O. Y. Osman, H. V. Kruis, Z. Nussinov, J. Tworzydlo, *Philos. Mag. B* **81**, 1485–1531 (2001).
18. H. V. Kruis, I. P. McCulloch, Z. Nussinov, J. Zaanen, *Phys. Rev. B Condens. Matter* **70**, 075109 (2004).
19. E. Haller *et al.*, *Nat. Phys.* **11**, 738–742 (2015).
20. L. W. Cheuk *et al.*, *Science* **353**, 1260–1264 (2016).
21. M. F. Parsons *et al.*, *Science* **353**, 1253–1256 (2016).
22. A. Omran *et al.*, *Phys. Rev. Lett.* **115**, 263001 (2015).
23. G. J. A. Edge *et al.*, *Phys. Rev. A* **92**, 063406 (2015).
24. P. T. Brown *et al.*, arXiv:1612.07746 [cond-mat.quant-gas] (22 December 2016).
25. M. Boll *et al.*, *Science* **353**, 1257–1260 (2016).
26. M. Endres *et al.*, *Science* **334**, 200–203 (2011).
27. See supplementary materials.
28. F. Woynarovich, *J. Phys. C Solid State Phys.* **15**, 85 (1982).
29. A. Imambekov, T. L. Schmidt, L. I. Glazman, *Rev. Mod. Phys.* **84**, 1253–1306 (2012).
30. J. Zaanen, *J. Phys. Chem. Solids* **59**, 1769–1773 (1998).
31. A. Recati, P. O. Fedichev, W. Zwerger, P. Zoller, *Phys. Rev. Lett.* **90**, 020401 (2003).
32. C. Kollath, U. Schollwöck, W. Zwerger, *Phys. Rev. Lett.* **95**, 176401 (2005).
33. M. Knap *et al.*, *Phys. Rev. Lett.* **111**, 147205 (2013).
34. E. W. Carlson, S. A. Kivelson, D. Orgad, V. J. Emery, *Concepts in High Temperature Superconductivity* (Springer Berlin Heidelberg, Berlin, Heidelberg, 2004), pp. 275–451.
35. Y. Zhang, E. Demler, S. Sachdev, *Phys. Rev. B* **66**, 094501 (2002).
36. T. Senthil, A. Vishwanath, L. Balents, S. Sachdev, M. P. A. Fisher, *Science* **303**, 1490–1494 (2004).
37. X.-G. Wen, *Quantum Field Theory of Many-Body Systems* (Oxford University Press, 2004).

ACKNOWLEDGMENTS

We acknowledge J. Koepsell and J. Vijayan for a critical reading of the manuscript and A. Sterdyniak and M. Zvonarev for useful discussions. Financial support was provided by the Max Planck Society (MPG) and European Union (UQUAM). F.G. and E.D. acknowledge support from Harvard–Massachusetts Institute of Technology Center for Ultracold Atoms (CUA), NSF grant DMR-1308435, the Moore Foundation, Air Force Office of Scientific Research (AFOSR) Quantum Simulation MURI, and AFOSR MURI Photonic Quantum Matter. The data that support the plots presented in this paper and other findings of this study are available from the corresponding author upon reasonable request.

SUPPLEMENTARY MATERIALS

www.sciencemag.org/content/357/6350/484/suppl/DC1
Supplementary Text
Figs. S1 to S5
References (*38*–*43*)

1 February 2017; accepted 6 July 2017
10.1126/science.aam8990

Revealing hidden antiferromagnetic correlations in doped Hubbard chains via string correlators

Timon A. Hilker, Guillaume Salomon, Fabian Grusdt, Ahmed Omran, Martin Boll, Eugene Demler, Immanuel Bloch and Christian Gross

Science **357** (6350), 484-487.
DOI: 10.1126/science.aam8990

Spin-charge separation in atomic chains

Strongly interacting electrons lined up along a string can experience the so-called spin-charge separation, where the electrons "split" into effective carriers of spin and charge, which then move independently. This phenomenon has been observed, somewhat indirectly, in solids. Hilker *et al.* show spin-charge separation in a direct way by using a one-dimensional (1D) array of cold atoms, playing the role of electrons, whose degrees of freedom of spin and charge can be monitored using a fermionic quantum gas microscope. Empty sites in the 1D lattice moved freely without disturbing the underlying antiferromagnetic order.

Science, this issue p. 484